THE JOURNAL OF BIOLOGICAL CHEMISTRY VOL. 289, NO. 2, pp. 814–826, January 10, 2014

Defining the Communication between Agonist and Coactivator Binding in the Retinoid X Receptor α Ligand Binding Domain*[S]

Received for publication, April 22, 2013, and in revised form, October 31, 2013 Published, JBC Papers in Press, November 1, 2013, DOI 10.1074/jbc.M113.476861

LeeAnn J. Boerma[‡], Gang Xia[§], Cheng Qui[§], Bryan D. Cox[§], Michael J. Chalmers[¶], Craig D. Smith[‖], Susan Lobo-Ruppert, Patrick R. Griffin[¶], Donald D. Muccio[§1], and Matthew B. Renfrow[‡2]**

*From the Departments of [‡]Biochemistry and Molecular Genetics, [§]Chemistry, [‖]Vision Sciences, and **Medicine, University of Alabama at Birmingham, Birmingham Alabama 35294 and the [¶]Department of Molecular Therapeutics, The Scripps Research Institute, Scripps Florida, Jupiter, Florida 33458*

Background: Some retinoid X receptor (RXR) agonists have potential as cancer drugs.
Results: Structures of RXR in complex with two different agonists show similar folds. Dynamics analysis reveals unique ligand-induced dynamics in helices 3, 11, and 12.
Conclusion: Two networks of interactions that connect RXR agonists to coactivator binding are defined.
Significance: Recognition of common conformational changes and distinguishing dynamics of RXR-selective agonists is necessary for advances in drug design.

Retinoid X receptors (RXRs) are obligate partners for several other nuclear receptors, and they play a key role in several signaling processes. Despite being a promiscuous heterodimer partner, this nuclear receptor is a target of therapeutic intervention through activation using selective RXR agonists (rexinoids). Agonist binding to RXR initiates a large conformational change in the receptor that allows for coactivator recruitment to its surface and enhanced transcription. Here we reveal the structural and dynamical changes produced when a coactivator peptide binds to the human RXRα ligand binding domain containing two clinically relevant rexinoids, Targretin and 9-*cis*-UAB30. Our results show that the structural changes are very similar for each rexinoid and similar to those for the pan-agonist 9-*cis*-retinoic acid. The four structural changes involve key residues on helix 3, helix 4, and helix 11 that move from a solvent-exposed environment to one that interacts extensively with helix 12. Hydrogen-deuterium exchange mass spectrometry reveals that the dynamics of helices 3, 11, and 12 are significantly decreased when the two rexinoids are bound to the receptor. When the pan-agonist 9-*cis*-retinoic acid is bound to the receptor, only the dynamics of helices 3 and 11 are reduced. The four structural changes are conserved in all x-ray structures of the RXR ligand-binding domain in the presence of agonist and coactivator peptide. They serve as hallmarks for how RXR changes conformation and dynamics in the presence of agonist and coactivator to initiate signaling.

Nuclear receptor (NR)[3] proteins are ligand-inducible transcription factors that up-regulate target genes. Ligand binding causes a major structural rearrangement of the ligand-binding domain (LBD) that exposes/buries key residues on the LBD surface for coactivator binding. Many coactivator proteins contain amphipathic helices with an L*XX*LL motif that bind the LBD to enhance gene expression. Corepressor proteins compete for this binding site and down-regulate target gene expression. Thus, NR signaling depends on two factors: the presence/absence on the NR agonist and the abundance of coactivators relative to corepressors. Understanding how NR agonists induce conformational changes to generate a surface on the LBD to recruit coactivator proteins and activate transcription is a central question remaining in NR signaling.

Vitamin A acids (retinoids) bind and activate two classes of NR proteins: the retinoic acid receptors (RARs) and retinoid X receptors (RXRs). When RXR was discovered, it was designated an orphan NR because its endogenous ligand was not identified (1). In 1992, 9cRA (Fig. 1) was proposed to be the high affinity ligand for RXR (2, 3). 9cRA bound to RXRs in the nanomolar range ($K_d \sim 10$ nM) and activated gene expression 40 times more potently than all-*trans*-retinoic acid, the high affinity ligand for RAR (2). 9cRA also binds/activates RAR, making it a pan-agonist for both RAR and RXR signaling pathways (4, 5). Moras and

* This work was supported, in whole or in part, by National Institutes of Health Grants 2 P50 CA089019 (to D. D. M.), 5 P50 CA089019 (to M. B. R.), RR17261 (to M. B. R.). This work was also supported by a grant from the Alabama Drug Discovery Alliance (to M. B. R.) and Komen Foundation Grant BCTR 20000690 (to D. D. M.).
[S] This article contains supplemental Tables S1 and S2.
The atomic coordinates and structure factors (codes 4K4J and 4K6I) have been deposited in the Protein Data Bank (http://wwpdb.org/).
[1] To whom correspondence may be addressed: Dept. of Chemistry, University of Alabama at Birmingham, 901 14th St. South, Birmingham, AL 35294. Tel.: 205-934-8285; Fax: 205-934-2543; E-mail: muccio@uab.edu.
[2] To whom correspondence may be addressed: Dept. of Biochemistry and Molecular Genetics, University of Alabama at Birmingham, 570 McCallum Basic Sciences Bldg., 1918 University Blvd., Birmingham, AL 35294. Tel.: 205-996-4681; E-mail: renfrow@uab.edu.

[3] The abbreviations used are: NR, nuclear receptor; RXR, retinoid X receptor; hRXRα, human retinoid X receptor α; LBD, ligand-binding domain; 9cUAB30, 9-*cis*-UAB30; 9cRA, 9-*cis*-retinoic acid; GRIP-1, glucocorticoid receptor-interacting protein-1; HDX, hydrogen/deuterium exchange; LBP, ligand binding pocket; H*n*, helix *n*; ITC, isothermal titration calorimetry; BisTris, 2-[bis(2-hydroxyethyl)amino]-2-(hydroxymethyl)propane-1,3-diol; %D, percentage of deuterium incorporation; RAR, retinoic acid receptor; RK3E cells, rat kidney epithelial cells; KLF4, Krüppel-like factor 4; Bis-Tris, 2-Bis(2-hydroxyethyl)amino-2-(hydroxymethyl)-1,3-propanediol.

co-workers (6) solved the x-ray structure of 9cRA bound to hRXRα-LBD. When compared with their structure of apo-hRXRα-LBD homodimer (7), they reported that Helix 12 (H12) and other residues at the carboxyl end of the LBD significantly changed confirmation moving from an extended position into the folded active conformation when agonist was bound (mouse trap model). However, HDX MS and NMR analyses of the agonist-bound RXRα-LBD without coactivator peptides firmly demonstrate that H12 remains dynamic rather than static as predicted in the mousetrap model (8–10). It has been demonstrated that HDX MS provides a better method for comparing how agonists that bind the same ligand binding pocket (LBP) in an NR produce changes in protein dynamics for proteins that undergo small conformational changes (8, 11).

Recently, we solved the x-ray crystal structure of hRXRα-LBD bound to 9cRA with a coactivator peptide, glucocorticoid receptor-interacting protein-1 (GRIP-1). These studies revealed the structural and dynamical rearrangements of H12 and other residues associated with coactivator binding to the holo-RXRα-LBD (12). In this structure, we observed four tertiary structural changes that connected the retinoid in the LBP to H12 residues. In each of these changes, residues moved from a solvent-exposed environment to one that interacts with residues on H12. Our HDX MS results revealed reduced dynamics in the protein backbone, which correlated with each of the four tertiary structural changes in the LBD. In fact, the changes in the crystal structures induced by coactivator binding were subtle compared with the significant reduction in dynamics of the peptides associated with these residues, which reside one layer away from the coactivator binding site and point toward the LBP of RXR. These studies provide a hypothesis for how 9cRA remolds the surface of the LBD to create a hydrophobic cleft to promote coactivator binding.

Based on these results, we were interested to explore if the structural and dynamical changes identified for coactivator binding to hRXRα-LBD containing the pan-agonist 9cRA are also present for hRXRα-LBD containing selective RXR agonists. There are numerous examples of RXR agonists that selectively enhance signaling through RXRs independent of RAR signaling. Targretin was discovered by the Dawson and Pfahl groups (SR-11247) as a potent rexinoid (13), and this rexinoid was translated to the clinic by Ligand Pharmaceuticals (14). Targretin shares little structural similarity with 9cRA (Fig. 1), but it does preserve the overall shape and polarity of 9cRA. Numerous studies have shown that Targretin is as effective as 9cRA in cancer prevention and therapy models (15–18). Human clinical trials revealed that Targretin was better tolerated than 9cRA and did not produce many of the classic retinoic acid-associated toxicities (except for hyperlipidemia) (19, 20).

To achieve even higher RXR selectivity, many groups, including our own, have designed tissue-selective rexinoids that can be administered for cancer prevention without exhibiting dose-limiting lipid toxicities. 9cUAB30 uses a tetralone ring to replace the trimethylcyclohexenyl ring of 9cRA (Fig. 1). Although 9cUAB30 is slightly less potent than Targretin or 9cRA, it displays a higher degree of RXR selectivity. 9cUAB30 has also been shown to be effective in cancer prevention models (21–25). 9cUAB30 is a tissue-selective RXR agonist; it does not act as an agonist in liver to activate lipid biosynthesis although it has agonist capabilities in cancer cells (26). A Phase I human clinical trial has shown that 9cUAB30 is well tolerated in human volunteers without lipid toxicity (27).

In this study, we compare the structural and dynamical changes in hRXRα-LBD homodimers due to binding of the coactivator peptide GRIP-1 when either Targretin or 9cUAB30 is present. We were particularly interested in observing if coactivator binding induces similar structural and dynamical changes in the hRXRα-LBD homodimers bound to a rexinoid as we observed for homodimers bound with the pan-agonist 9cRA. Is there a common set of structural and dynamical changes characteristic of potent RXR agonists, and which changes (if any) are dependent on the type of rexinoid present in the LBD (rexinoid-specific changes)?

EXPERIMENTAL PROCEDURES

Materials—9cUAB30 was synthesized at the University of Alabama at Birmingham according to previous methods (21, 24). Targretin was provided by Dr. Clinton Grubbs at UAB. A 13-mer peptide derived from residues 686–698 of GRIP-1 was synthesized by AnaSpec Inc. (KHKILHRLLQDSS) with a molecular mass of 1575.9 Da. The structures and purity of the rexinoids and peptide were confirmed by NMR and LC-MS. The concentration of peptide was determined by ^{1}H NMR added to a known concentration of tryptophan as reported previously (12).

Oncogenic Transformation Assay—The oncogenic transformation was performed as described previously by Jiang *et al.* (28). Cells infected with KLF4-ER were given DMEM supplemented with 4-hydroxytamoxifen (0.3 μM; Calbiochem) and 9cRA, 9cUAB30, Targretin, or vehicle (DMSO) every other day performed in duplicate for each concentration. Three weeks postinfection, transformed foci were fixed, stained, and counted and compared against the DMSO control.

Protein Expression and Purification—The protein expression and purification of hRXRα-LBD (Thr^{223}–Thr^{462}) was accomplished according to Egea and Moras (29) and Xia *et al.* (12). Briefly, the His_6-tagged hRXRα-LBD fusion protein was expressed in BL21-(DE3) *Escherichia coli* bacteria (Invitrogen), which was grown in Luria broth (LB) medium at 20 °C. Protein expression was induced with 1 mM isopropyl-β-D-thiogalactopyranoside. Cells were lysed using a French press (1500 p.s.i.) and then centrifuged at 25,000 rpm for 30 min. The His_6-tagged hRXRα-LBD was eluted from a nickel-chelating column (GE Healthcare) using a 20 mM Tris (pH 8.0) buffer containing 300 mM imidazole and 500 mM NaCl. The eluted hRXRα-LBD fractions were dialyzed in a 10 mM Tris buffer (pH 8) containing 50 mM NaCl, 0.5 mM EDTA, and 2 mM DTT. The His_6 tag was hydrolyzed using α-thrombin (Novagen, Madison, WI) at 4 °C. The hRXRα-LBD homodimers were separated at 4 °C from tetramers using a HiLoad Superdex 75 gel filtration column (GE Healthcare) with a 1.0 ml/min flow rate. SDS-PAGE and MALDI mass spectrometry were used to establish a purity of >97% and mass of the monomers (m/z = 26,433.1 Da). Native PAGE confirmed that the isolated fractions were hRXRα-LBD homodimers.

TABLE 1
Crystallographic data collection and refinement statistics for hRXRα-LBD complexes

	9cUAB30	Targretin
Data collection		
Unit cell parameters (Å)	$a = 66.04$, $b = 66.04$, $c = 111.16$	$a = 68.15$, $b = 68.15$, $c = 106.59$
Unit cell parameters (degrees)	$\alpha = 90$, $\beta = 90$, $\gamma = 90$	$\alpha = 90$, $\beta = 90$, $\gamma = 90$
Space group	$P4_32_12$	$P4_32_12$
Resolution (last shell) (Å)	29.53–2.00 (2.07–2.00)	29.30–2.10 (2.18–2.10)
No. of total/unique reflections	93,556/17,180	124,225/15,301
R_{merge} (last shell) (%)	0.048 (0.322)	0.078 (0.350)
Redundancy (last shell)	5.45 (4.47)	8.12 (7.73)
Completeness (last shell) (%)	99.5 (99.1)	100.0 (99.7)
I/σ (last shell)	17.3 (4.6)	14.1 (4.5)
Refinement		
No. of residues	223	223
No. of protein atoms	1789	1789
No. of water molecules	115	71
No. of ligand atoms	22	26
R_{cryst} (%)	23.95	24.62
R_{free} (%)	28.31	28.87
Root mean square deviation deviation from ideality		
Bond length (Å)	0.0068	0.0091
Bond angles (degrees)	1.089	1.162
Ramachandran plot, residues in		
Most favored regions (%)	94.98	95.89
Additional allowed regions (%)	3.65	3.20
Generously allowed regions (%)	1.37	0.91
Average *B* factor (Å^2)	37.33	43.04
Non-hydrogen protein atoms (Å^2)	37.23	43.31
Non-hydrogen ligand atoms (Å^2)	36.73	30.19
Water molecules (Å^2)	38.96	40.92

Crystallization of hRXRα-LBD Homodimers Bound to 9cUAB30/Targretin and to GRIP-1—Manipulation of 9cUAB30 and Targretin was performed under dimmed red light due to light sensitivity of the compounds. Crystallization of hRXRα-LBD·9cUAB30·GRIP-1 and hRXRα-LBD·9cRA·GRIP-1 homodimer complexes was similar to the method described previously (12) and those reported by Moras and co-workers (30). The crystals of hRXRα-LBD homodimers with 9cUAB30 were obtained in a reservoir solution containing 5–10% PEG 4000, 2–5% glycerol, 0.1 M BisTris at pH 7.0. The crystals of the hRXRα-LBD containing Targretin and GRIP-1 formed more slowly than those for 9cUAB30. An additional microseeding step was applied by transferring tiny crystals of the complex into a new crystallization reservoir. X-ray quality crystals of the hRXRα-LBD·Targretin·GRIP-1 complex were obtained at 5–15% PEG 4000, 6–12% glycerol, 0.1 M BisTris at pH 7.0. Both crystals had a $P4_{(3)}2_{(1)}2$ space group, which was the same as the crystals of the hRXRα-LBD complex with 9cRA and GRIP-1 reported in our previous paper (12).

Data Collection, Structure Determination, and Refinement—Diffraction data of these two crystals were collected using the Rigaku R-AXIS IV+ at the Center for Biophysical Sciences and Engineering at the University of Alabama at Birmingham or an R-AXIS IV++ at BioCryst. Inc. Data collection, structure determination, and refinement strategy were described in detail previously (12). A summary of the diffraction data and crystal structure refinement statistics is given in Table 1. The contacts between hRXRα-LBD and rexinoid (either 9cUAB30 or Targretin) were determined by ligand-protein contacts (31). Contacts between GRIP-1 and hRXRα-LBD were determined by contacts of structural units (31). VOIDOO (32) and MAPMAN (33) programs were used for determining the LBP.

Isothermal Titration Calorimetry of GRIP-1 Binding to Holo-hRXRα-LBD—A VP-Isothermal titration calorimeter (Microcal, Piscataway, NJ) was used to measure binding of the GRIP-1 coactivator peptide to holo-hRXRα-LBD homodimers as described previously (12). Each titration experiment consisted of 30 injections of 8 μl of GRIP-1 peptide (0.04–0.12 mM) into the sample cell containing 1.34 ml of hRXRα-LBD homodimers (0.05 mM) in 10 mM Tris buffer (pH 8.0) containing 50 mM NaCl, 0.5 mM EDTA, and 2 mM DTT. 9cUAB30 and Targretin were dissolved in DMSO and added at a ratio of 2:1 (retinoid/protein). Both retinoid solution and hRXRα-LBD solution were degassed at least 15 min before the retinoids were added to the protein solution. The isothermal calorimetry (ITC) data were processed using the ORIGIN 7 software. The titration curves were fit to a single site binding model by a nonlinear least squares method. The ITC experiments were performed at 20, 25, and 30 °C, and the heat capacity change was found by linear regression of the corrected enthalpies *versus* temperature.

Automated Hydrogen Deuterium Exchange Experiments—Solution phase H/D exchange experiments were performed using an automated LEAP Technologies Twin PAL HTS autosampler (LEAP Technologies, Carrboro, NC) (8). In short, 40 pmol of hRXR-LBD homodimer in the presence of 10 times the concentration of ligand or vehicle (DMSO) and GRIP-1 coactivator peptide (>95% saturation) were dispensed into a mixing tray and diluted with 16 μl of deuterated buffer or protonated buffer for control experiments. Following on-exchange periods (4 °C), the entire sample was picked up and dispensed into 30 μl of quench buffer (3 M urea, 1% TFA, 50 mM TCEP, 1 °C). Samples were taken at 10, 30, 60, 300, 900, and 3600 s and performed in triplicate. Samples were digested for 2.5 min on an in-house prepared pepsin column (1 °C). Sample loading,

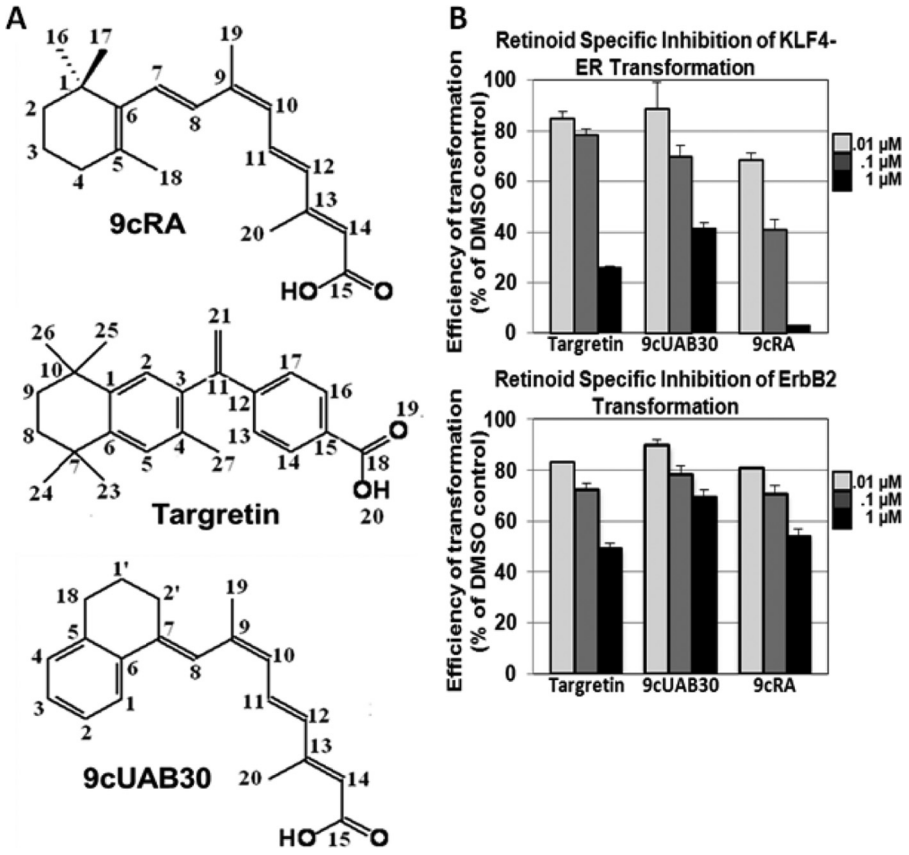

FIGURE 1. **9cRA, Targretin, and 9cUAB30 prevent oncogenic transformation in epithelial cells.** *A*, the structures and numbering schemes of 9cRA, Targretin, and 9cUAB30. *B*, percentage of oncogenic transformation of epithelial cells treated with 9cRA, Targretin, or 9cUAB30 relative to DMSO controls. *Top right*, KLF4-ER tamoxifen-induced oncogenic transformation; *bottom right*, ErbB2-ER tamoxifen-induced oncogenic transformation. *Error bars*, S.D.

digestion, and desalting were driven with an isocratic HPLC pump at 200 μl min^{-1}. Peptic peptides were then loaded onto a desalting C8 phase trap column (3.5 μM; Agilent), followed by the analytical column (50 mM × 2.1, 5 μM; Thermo Scientific). Eluent was injected into the instruments at 50 μl min^{-1}, and spectra were acquired over the scan range of 200–2000 *m*/*z*. Each spectrum was the sum of two microscans. HDX MS raw files were processed and visualized by use of the HD Desktop software (34). Differential HDX perturbation values were calculated by taking the averaged differences in deuterium incorporation for five on-exchange time points from the deuterium incorporation of the reference, apo-hRXRα-LBD·GRIP-1. HDX perturbations greater than ±5% were considered significant as described previously (8, 12). For identification of discriminatory dynamics of individual HDX MS peptides between the three agonists, changes in the measured percentage of deuterium incorporation (%D) relative to the apo control were compared at the 30 s or 30 min time points. Statistically significant differences were determined by use of a two-tailed *t* test as described previously (11).

Peptide Sequencing—Proteolytic digestion prior to mass spectromic analysis allowed regional monitoring of deuterium incorporation. Identification of hRXRα-LBD peptides was achieved by use of positive ion electrospray ionization LC tandem mass spectrometry (MS/MS) on a hybrid linear quadrupole ion trap 7 Tesla Fourier transform ion cyclotron resonance mass spectrometer (Thermo Fisher Scientific). Pilot experiments optimized protein digestion conditions, and peptides were identified by data-dependent tandem LC MS/MS as described previously (35).

RESULTS

In Vitro Analysis of RXRα Agonist Anticancer Properties—Previous reports have shown that 9cRA, Targretin, and 9cUAB30 are potent agonists of RXRα transcription (2, 14, 21). Here we compared each RXR agonist for its capacity to inhibit oncogenic transformation of rat kidney epithelial (RK3E) cells. In this assay, oncogenic transformed RK3E epithelial cells form dense foci surrounded by contact-inhibited parental cells in the absence of retinoid (28, 36–42). For this study, the RK3E cells were transduced with retrovirus encoding a conditional, 4-hydroxytamoxifen-inducible Krüppel-like factor 4 (KLF4) allele (KLF4-ER) (43), ErbB2, or empty vector as the control. When the cells were dosed with three different concentrations of retinoid every other day for 3 weeks, formation of foci was significantly decreased in either ErbB2- or KLF4-ER-infected RK3E cells relative to DMSO controls in a dose-dependent manner (Fig. 1). Targretin was more effective than 9cUAB30 at the highest dose (75% *versus* 59%), which correlated with its potency as an RXR agonist. The pan-agonist 9cRA was the most effective retinoid tested (95%), but this pan-agonist can inhibit oncogenesis by activating both RAR and RXR signaling pathways.

TABLE 2
Summary of ITC measurements of GRIP-1 to hRXRα-LBD·retinoid complexes

Temperature	K_a	ΔH	$-T\Delta S$	ΔG	n	ΔC_p
°C	μM^{-1}	kcal/mol	kcal/mol	kcal/mol		cal mol^{-1} K^{-1}
Targretin						
20	1.80 ± 0.07	−7.18 ± 0.03	−1.21 ± 0.06	−8.39 ± 0.03	0.96	−413 ± 25
25	1.59 ± 0.04	−9.46 ± 0.02	0.84 ± 0.04	−8.62 ± 0.02	0.96	
30	1.25 ± 0.04	−11.31 ± 0.03	2.86 ± 0.06	−8.45 ± 0.03	0.97	
9cUAB30						
20	1.62 ± 0.06	−7.12 ± 0.02	−1.21 ± 0.04	−8.33 ± 0.02	1.06	−356 ± 29
25	1.33 ± 0.04	−8.88 ± 0.03	0.52 ± 0.06	−8.36 ± 0.03	1.05	
30	0.95 ± 0.02	−10.68 ± 0.02	2.39 ± 0.04	−8.29 ± 0.02	1.05	
9cRA						
20	2.15 ± 0.07	−6.78 ± 0.02	−1.71 ± 0.04	−8.49 ± 0.02	0.98	−401 ± 18
25	1.81 ± 0.06	−9.15 ± 0.03	0.61 ± 0.06	−8.54 ± 0.03	0.92	
30	1.38 ± 0.03	−11.13 ± 0.03	2.61 ± 0.06	−8.52 ± 0.03	0.95	

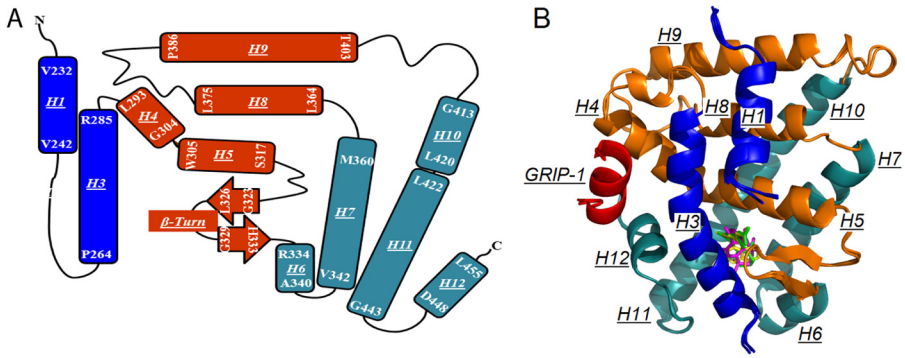

FIGURE 2. **X-ray crystal structures of hRXRα-LBD bound to either Targretin, 9cUAB30, or 9cRA and GRIP-1.** *A*, topology map of holo-hRXRα-LBD showing a three-sandwich helical fold. H4, H5, H8, H9, and the β-sheet (*orange*) are sandwiched by H1, H2 (missing), and H3 (*blue*) at one side and H6, H7, H10, and H11 (*dark cyan*) at the other side. *B*, overlay of three hRXRα-LBD·GRIP-1·agonist structures. Helices are rendered in the same *colors* as in *A*; GRIP-1 is shown in *red*.

Binding Affinity of GRIP-1 with hRXRα-LBD Containing 9cUAB30 or Targretin—ITC was used to measure the thermodynamics of GRIP-1 binding to hRXRα-LBD containing either 9cUAB30 or Targretin at 20, 25, and 30 °C (Table 2). As observed for 9cRA complexes in our previous analysis (12), the binding stoichiometry was nearly 1:1 (coactivator peptide/LBD monomer unit). The free energy of GRIP-1 binding to the hRXRα-LBD complexes containing rexinoid was driven strongly by a large negative enthalpy change, and it is opposed by entropy although the coactivator peptide contains the L*XX*LL motif (Table 2). The magnitude of this thermodynamic signature was very similar for homodimers containing rexinoid (9cUAB30 or Targretin) or pan-agonist (9cRA) in its LBP (Table 2) (12). Using the temperature dependence of the enthalpy change for binding, the heat capacity changes for GRIP-1 binding to the hRXRα-LBD homodimers containing rexinoid were determined. The heat capacity changes were very similar for Targretin and 9cRA complexes (−401 ± 18 cal mol^{-1} K^{-1} and −413 ± 25 cal mol^{-1} K^{-1}), and it was slightly smaller for 9cUAB30 complex (−356 ± 29 cal mol^{-1} K^{-1}).

Comparisons of the X-ray Crystal Structures of hRXRα-LBD Homodimers Bound to RXR Agonists and GRIP-1—To explore the structures of this NR with different rexinoids and a coactivator peptide, we crystallized hRXRα-LBD homodimers bound with the GRIP-1 coactivator peptide and either 9cUAB30 or Targretin. Both crystal structures belonged to the $P4_{(3)}2_{(1)}2$ space group, and each asymmetric unit contained two monomers with GRIP-1 bound to each monomer. The structures were determined to 2.0 Å resolution for the hRXRα-LBD·9cUAB30·GRIP-1 (4K4J) complex and 2.25 Å resolution for the hRXRα-LBD·Targretin·GRIP-1 complex (4K6I) by use of the molecular replacement method (Table 1). Each structure had identical two-dimensional topology (Fig. 2*A*). This LBD formed a three-layer helical sandwich with H1 and H3 on one side and H6, H7, H10, H11, and H12 on the other (Fig. 2). The x-ray structures of hRXRα-LBD bound with either Targretin or 9cUAB30 and GRIP-1 were overlaid onto the structure of hRXRα-LBD·9cRA·GRIP-1 (12). The overlay showed that the hRXRα-LBD backbone atoms of these three crystal structures were very similar (Fig. 2*B*). The root mean square deviation was 0.137 Å for the 229 backbone residues of hRXRα-LBD·9cUAB30 (4K4J *versus* 3OAP), and it was 0.210 Å for hRXRα-LBD·Targretin (4K6I *versus* 3OAP).

GRIP-1·Holo-hRXRα·LBD Contacts—GRIP-1 coactivator peptide contains 13 residues (^{686}KHKILHRLLQDSS^{698}), including one L*XX*LL motif. In both structures, GRIP-1 adopted a two-turn amphipathic helix (Fig. 3*A*) and was positioned in the coactivator binding site of hRXRα-LBD formed by H3, H4, and H12 (12, 30). The helical conformation of GRIP-1 and the interactions of the coactivator peptide with hRXRα-LBD were nearly identical in these two structures (Fig. 3*B*). The hydrophobic surface of the amphipathic peptide (Ile^{689}, Leu^{690}, Leu^{693}, and Leu^{694}) interacted with a hydrophobic binding pocket on the surface of the LBD (Fig. 3*B*). There were subtle differences in the manner in which GRIP-1 interacted with the surface of the hRXRα-LBD (Fig. 3*B*). When Targretin occupied the LBP, the hydrophobic contact between Ile^{689} of GRIP-1 and Thr^{449} (H12) of hRXRα-LBD was smaller (4.8 and 17.5 $Å^2$) compared with the same

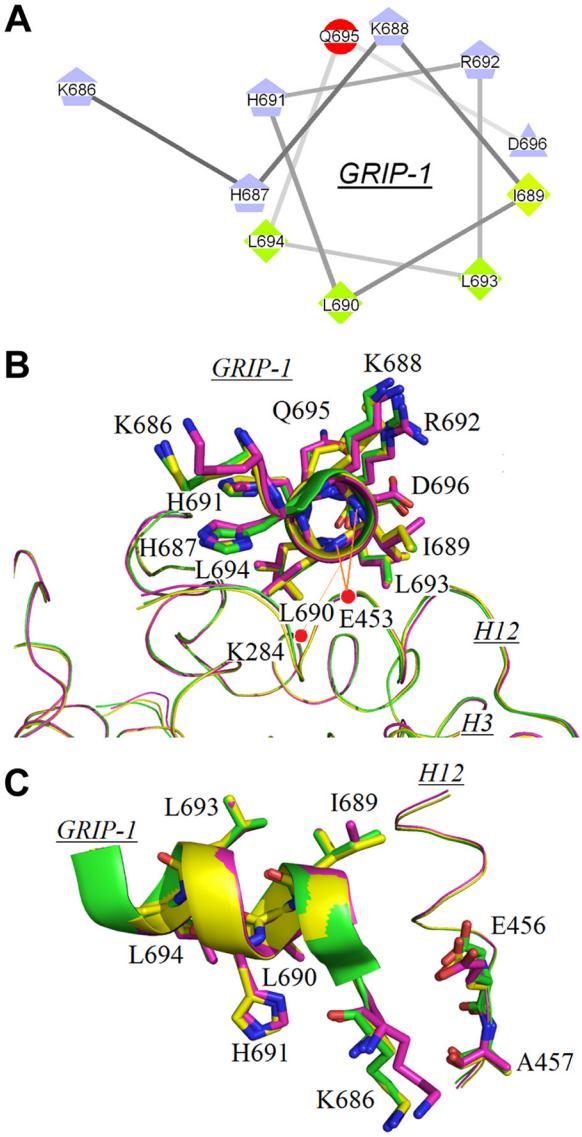

FIGURE 3. **Interactions of the coactivator peptide GRIP-1 with surface residues on holo-hRXRα-LBD.** *A*, *helical wheel view* of GRIP-1 bound to holo-hRXRα-LBD illustrates its amphipathic character. *B*, overlay of GRIP-1 in holo-hRXRα-LBD structures containing 9cRA (*green*), 9cUAB30 (*yellow*), and Targretin (*magenta*). Two charge clamps between GRIP-1 and hRXRα-LBD are indicated by *red dashed lines*. *C*, *side view* of GRIP-1 binding to LBD showing relative positions of Glu^{456} and Ala^{457} on H12 of hRXRα-LBD to Lys^{686} on GRIP-1. The *color code* is the same as in *B*.

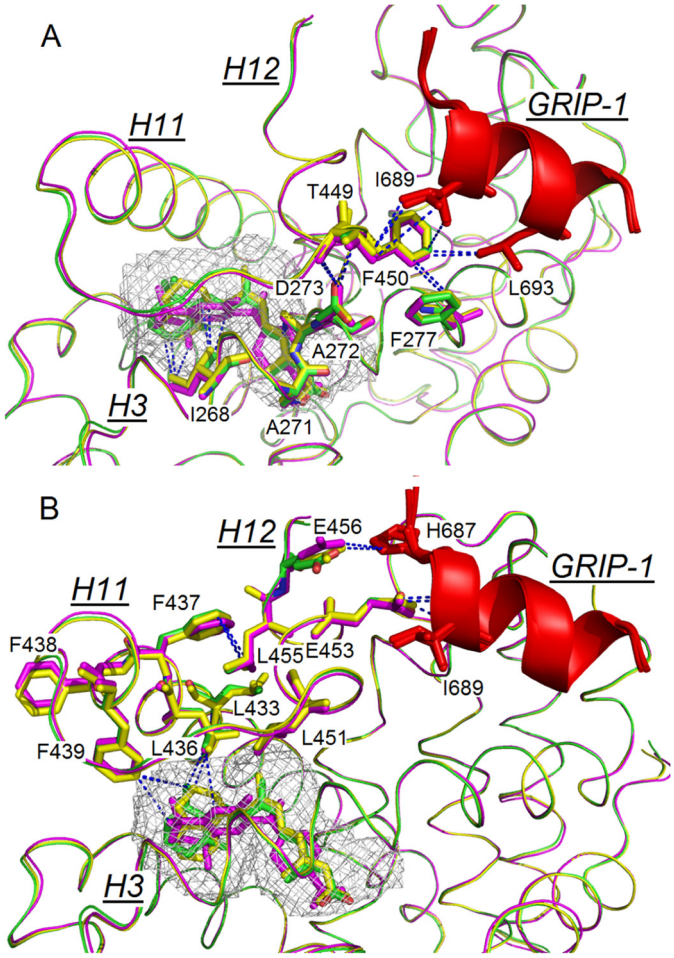

FIGURE 4. **Networks of interacting residues between the GRIP-1 (*red*) and H3, H11, and H12 of the holo-hRXRα-LBD containing 9cRA (*green*), 9cUAB30 (*yellow*), and Targretin (*magenta*).** *Blue dashed lines* link interacting residues. *A*, network between retinoid ring, H3 residues, H12 residues, and GRIP-1. *B*, network between retinoid ring, H11 residues, H12 residues, and GRIP-1.

interaction when 9cUAB30 (3.5 and 45.5 $Å^2$) or 9cRA (3.6 and 46.0 $Å^2$) was present. The sec-butyl group of Ile^{689} changed conformations in the Targretin-bound structure. Additionally, Lys^{686} of GRIP-1 interacted with Glu^{456} and Ala^{457} (C terminus) of the hRXRα-LBD when Targretin was present, but this interaction was weaker when 9cRA or 9cUAB30 was bound (Fig. 3*C*). Last, the imidazole group of His^{691} of GRIP-1 shifted slightly toward the carboxylate group of Asp^{295} (H4) when Targretin was bound to the LBD. The contact surface area between His^{691} in GRIP-1 and H4 residues (Leu^{294}, Asp^{295}, Val^{298}) was 20% less when Targretin was bound (56.7 $Å^2$) relative to when 9cUAB30 (71.9 $Å^2$) or 9cRA (81.4 $Å^2$) was bound.

Structural Changes Induced by GRIP-1 Binding—The structural changes induced by GRIP-1 binding to hRXRα-LBD when either Targretin or 9cUAB30 was bound to the LBD were compared with those of hRXRα-LBD·9cRA (Protein Data Bank code 1FBY) and to hRXRα-LBD·9cRA·GRIP-1 (3OAP). In the two crystal structures containing rexinoid and GRIP-1, Phe^{277} formed a π-hydrogen bond with Phe^{450} (Fig. 4*A*). This interaction was found in 3OAP but absent in 1FBY. Phe^{277} (H3) and Phe^{450} (H12) also interacted with two hydrophobic residues of GRIP-1 (Ile^{689} and Leu^{693}). The carboxylate group of Asp^{273} (H3) formed hydrogen bonds to the backbone amide nitrogens of Phe^{450} and Thr^{449}, which are both on H12 (Fig. 4*A*). H3 contains three nonpolar residues (Ile^{268}, Ala^{271}, and Ala^{272}), which form the LBP and are on the opposite side of the H3 from Asp^{273} (Fig. 4*A*). These interactions are displayed by *blue dashed lines* in Fig. 4*A*. These interactions provide a molecular bridge between the coactivator peptide binding sites and carboxylate end of the retinoid.

A second molecular bridge was identified that connects the coactivator peptide to the nonpolar retinoid rings. At the surface of NR, two glutamates on H12 (Glu^{453}/Glu^{456}), which were solvent-exposed in 1FYB, interacted with GRIP-1. Glu^{453} (H12) formed ionic interactions with the amides on the N terminus of GRIP-1 and is part of the charge clamp (44) (Figs. 3*B* and 4*B*).

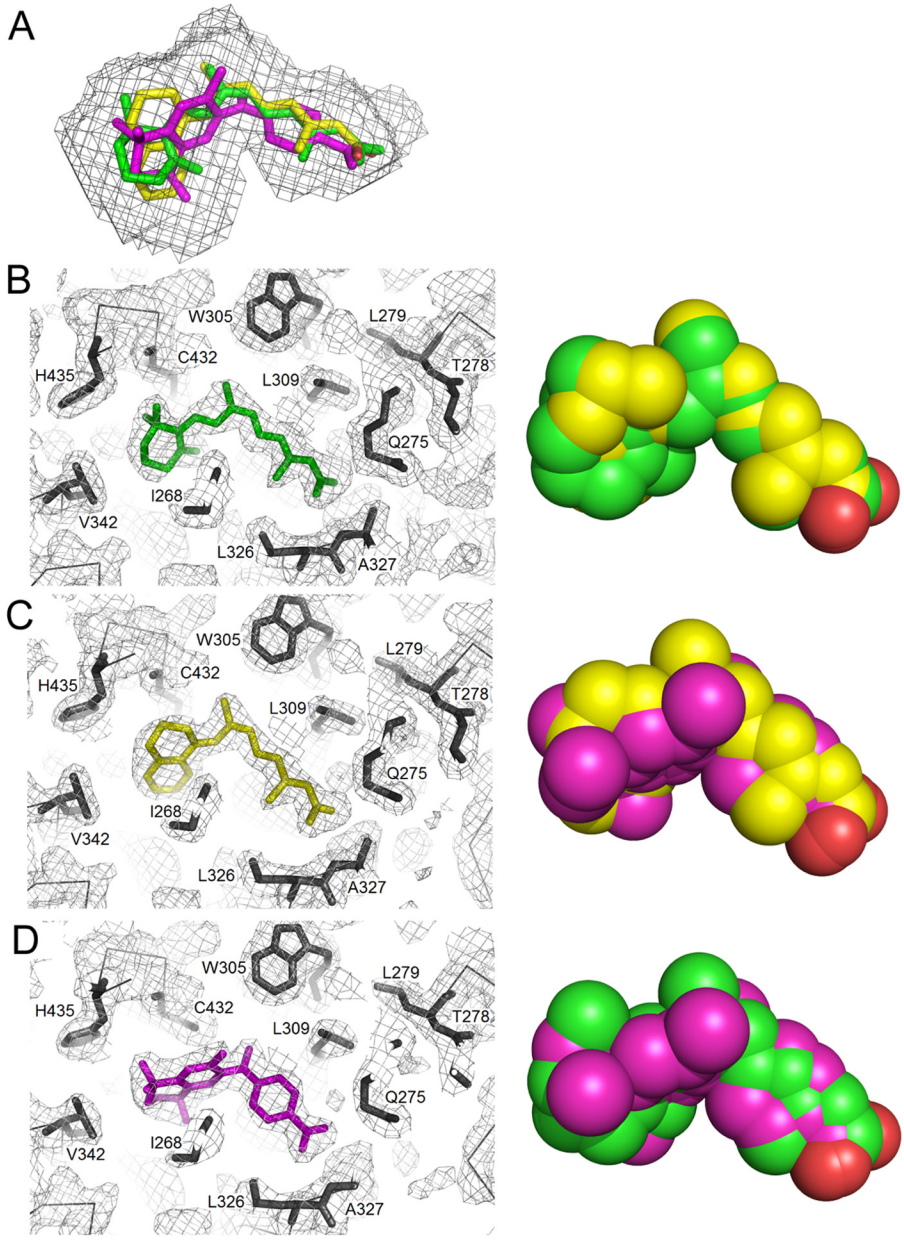

FIGURE 5. **Conformation of rexinoids and 9cRA in the ligand binding pocket of holo-hRXRα-LBD.** *A*, overlay of 9cRA (*green*), 9cUAB30 (*yellow*), and Targretin (*magenta*) in the ligand binding pocket. Shown are electron density maps ($2F_o - F_c$) for the retinoid binding pocket of hRXRα-LBD. *B*, 9cRA; *C*, 9cUAB30; *D*, Targretin. To the *right* of each electron density map, a *space-filling rendering* of each retinoid is given with one of the other retinoids overlaid.

Glu^{456} (H12) also contributed to this charge clamp by interacting with the side chain of His^{687} on GRIP-1 (Fig. 4*B*). The guanidinium group of the highly conserved Arg^{302} on H4 (45) formed strong hydrogen bonds with the backbone amides of Glu^{453} and Glu^{456} (~3.2 Å). These interactions were identical to what was found previously (12). GRIP-1 binding reoriented Phe^{437} (H11) inward so that it was now capable of interacting with Leu^{455} of H12 (Glu^{453} and Glu^{456} are on the opposite face of H12 from Leu^{455}). Phe^{437} (H11) changed conformations and pointed toward H12 so that the phenyl side chain is within van der Waals contact with the *iso*-butyl group of Leu^{455} (H12). Leu^{455} (H12) is one of four leucine residues (with Leu^{451} (H12), Leu^{436} (H11), and Leu^{433} (H11)) that form a hydrophobic core between H11 and H12. A leucine hydrophobic core is one layer deeper from the surface of coactivator binding (Fig. 4*B*). Phe^{439}, Leu^{436}, and Leu^{451} make direct contacts to the retinoid rings of 9cRA, Targretin, and 9cUAB30.

Differences in the Ligand-Protein Contacts of Targretin/9cUAB30/9cRA Bound to hRXRα-LBD—We next examined the conformation of the retinoids in the LBP. Electron density maps clearly showed the presence of 9cUAB30 and Targretin in the LBP of hRXRα-LBD. Both retinoids adopted nonplanar, L-shaped conformations that fit well into the LBP (Fig. 5*A*). For 9cUAB30, the C8–C9 bond (C7-C8-C9-C10 torsional angle 121°) was twisted in a right-handed screw sense (Fig. 5*C*). For Targretin, the twist occurred about the C3–C11 bond (C2-C3-C11-C12 torsional angle −85°). In contrast, 9cRA twisted about the C6–C7 bond linking the polyene chain to the trimethylcyclohexenyl ring (C5-C6-C7-C8 torsional angle −14°). In each case, the twisted conformation of the retinoid relieved steric

repulsion between methyl groups. Each of three achiral retinoids adopted a right-handed screw sense in the LBP when viewed from the retinoid ring toward the carboxylate group down the long axis of the rexinoid.

The LBP of hRXRα-LBD is formed by residues contributed from H1, H3, H5, H7, H9, H11, H12, and the short two-turn β-sheet (6). The LBP is comprised of mainly hydrophobic residues and a few hydrophilic ones centered on the two-turn β-sheet and H5. The LBP of hRXRα-LBD bound to 9cRA and coactivator peptide GRIP-1 was formed by 34 residues, and its volume was 493 Å^3 (12). 9cRA (300 Da) occupied 371 Å^3 of the pocket volume (75% occupancy). In the structures reported here for the two rexinoids bound to hRXRα homodimers and GRIP-1, the LBPs were both slightly smaller (442 Å^3 for 9cUAB30; 456 Å^3 for Targretin) than that found for 9cRA. Thus, Targretin and 9cUAB30 filled this volume more than 9cRA (84% occupancy for Targretin; 78% occupancy for 9cUAB30).

In the 9cRA or rexinoid structures, the LBPs were formed by the same 24 residues (Fig. 5, compare *B*, *C*, and *D*). The elongated pockets (~16.8 Å) were lined with the 16 hydrophobic residues. Four H3 residues (Ile^{268}, Cys^{269}, Ala^{271}, and Ala^{272}) and four H7 residues (Val^{342}, Ile^{345}, Phe^{346}, and Val^{349}) formed the lower part of the LBP (Fig. 4*B*). Four H5 residues (Trp^{305}, Asn^{306}, Leu^{309}, and Phe^{313}) and four H11 residues (Cys^{432}, His^{435}, Leu^{436}, Phe^{439}) formed the other side of the pocket. The total contact surface area of the ligand-protein contacts between this portion of 9cUAB30 and H3 and H5 residues was very similar. Although 9cUAB30 contains a structurally different ring from 9cRA, the total surface area of the contacts was similar (12). The overlaid conformations of space-filled renderings of these two agonists were very similar (Fig. 5*B*).

The structure of Targretin in the LBP was more highly twisted than either 9cRA or 9cUAB30. When a space-filled overlay was made, C27 of Targretin occupied space in the LBP that 9cUAB30 or 9cRA did not (Fig. 5, *C* and *D*). The C24, C26, and C27 methyl groups of Targretin interacted more strongly with residues on H3 and H7 than 9cRA or 9cUAB30. The total surface area for the contacts between the ring carbons on Targretin and H3 and H7 residues increased by about 30 and 20 Å^2, respectively, over those found for the other two agonists. In contrast to H3 and H7, the interactions between Targretin and the residues on H11 decreased by 20 Å^2 relative to what was observed in 9cRA. The single structural change in the Targretin LBP *versus* that of 9cRA occurs at Cys^{432}. In the Targretin structure, the thiol group was rotated by about 116° and now points toward the C4 methyl group (4.6 Å away). Changes also occurred closer to the middle of the structure. The methylene C21 of Targretin formed a new contact to Ile^{310} on H5 (17 Å^2; 4.0 Å), which was a protein residue that does not interact directly to 9cRA or 9cUAB30.

HDX MS Analysis of hRXRα-LBD Complexes—Several differential HDX MS studies have shown that the dynamics of hRXRα-LBD change when agonist binds (8, 10, 12, 46). We also observed that GRIP-1 reduced deuterium incorporation of apo-hRXRα-LBD in the absence of agonist (12). Here we performed differential HDX MS analysis using apo-hRXRα-LBD·GRIP-1 as the reference control to address the question of whether rexinoid binding produced distinct hRXRα-LBD HDX exchange rates in the presence of GRIP-1. Ninety-seven peptides comprising 99% of hRXRα-LBD (<2 ppm error) were followed by HDX MS (supplemental Table S1). The %D was calculated for each peptide at each time point in triplicate by comparison with a no deuterium control (11). Overall changes in %D were examined across all time points relative to the apo-hRXRα-LBD-GRIP-1 reference. Additionally, individual HDX MS peptides were examined at the 30 s and/or 30 min time points to identify statistically significant differences in individual peptide %D between the hRXRα agonists.

The addition of rexinoids to the NR LBD complex in the presence of GRIP-1 reduced deuterium incorporation in peptides from H2, H3, β-sheet-H6, H7, H11, and H12. For peptides spanning H2, the β-sheet-H6, and H7, the change in %D was negative, and the extent of reduction was the same regardless of which rexinoid was bound to the homodimer. For example, the change in %D for the β-sheet peptide Leu^{326}–Gly^{343} was -8 ± 1% at 30 s regardless of agonist bound to the hRXRα-LBD (Fig. 6). Results for all overlapping H2 and H7 peptides followed this same pattern (supplemental Table S1). For the majority of LBD HDX MS peptides, Targretin and 9cUAB30 binding mimicked the changes in %D of 9cRA binding in the presence of GRIP-1. The list of all changes in %D is provided in supplemental Table S1.

For 15 (of 97) peptides, the overall reduction in %D was 10% or more. These HDX MS peptides encompassed three regions within the hRXRα-LBD and show statistically significant dynamics upon binding of Targretin, 9cUAB30, or the pan-agonist 9cRA. Four of the peptides included H3 residues, 10 peptides spanned the longer H11 and a C-terminal adjacent loop, and a single peptide included H12 residues. Fig. 6 shows representative %D *versus* time comparative HDX MS plots from these 15 peptides, including the H3 peptide Ala^{271}–Ala^{278}, H11 peptide Pro^{423}–Phe^{438}, and H12 peptide Phe^{450}–Met^{454} when bound to each ligand. Significantly, the overall reduction in %D was different for each of the agonists in these three areas, with the two rexinoids showing more reduction in %D for H3 (Targretin, −46%; 9cUAB30, −50%), H11 (Targretin, −32%; 9cUAB30, −28%), and H12 (Targretin, −11%; 9cUAB30, −12%) compared with 9cRA (H3, −26%; H11, −14%; H12, 1%). The overlapping peptides for H3 and H11 showed the same trend (supplemental Table S1). Fig. 6 also includes an H4 peptide as an example of an HDX MS peptide that does not change in %D in the presence of ligand, whether it is the two rexinoids or the pan-agonist 9cRA.

To determine if these comparative HDX MS differences for individual peptides were significant, we examined individual time points for each data set relative to their matched controls of unbound ligand. Chalmers *et al.* (11) have demonstrated that comparison of statistically significant differences in individual peptides %D at a single time point can be used to delineate between NR agonists based on their %D signatures. Fig. 6*B* provides this comparison for the four peptides in *A*. The change in %D for in H3, H11, and H12 when bound to either rexinoid showed statistically significant differences ($p < 0.0001$) compared with the same peptides when 9cRA was bound to the hRXRα-LBD in the presence of GRIP-1. There was no signifi-

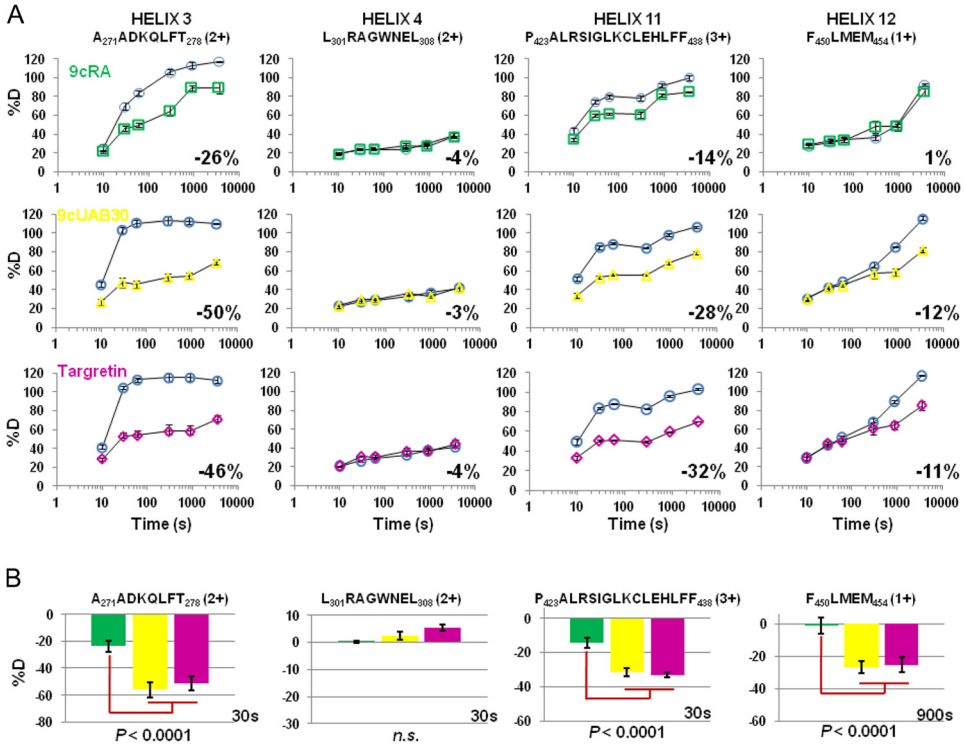

FIGURE 6. **HDX MS deuterium incorporation plots for hRXRα-LBD H3, H4, H11, and H12 peptic peptides (sequence indicated at the *top*).** *A*, %D is plotted *versus* a log time scale for each peptide. The rexinoids (Targretin and 9cUAB30) show distinct changes in %D compared with the pan-agonist 9cRA in the H3, H11, and H12 regions but not in H4. Shown is HDX MS analysis of hRXRα-LBD in the presence of retinoid and GRIP-1 (9cRA (*green squares*), 9cUAB30 (*yellow triangles*), and Targretin (*magenta diamonds*)) relative to the controls of the digested LBD without retinoid but with GRIP-1 (*blue circles*). *B*, comparison of individual time points (30 or 900 s) for the same four HDX MS peptides shows that the changes in %D for the H3, H11, and H12 peptides when the two rexinoids are bound (9cUAB30 (*yellow*) and Targretin (*magenta*)) are statistically significant relative to the same peptide when 9cRA (*green*) is bound to the hRXRα-LBD. *Error bars*, S.D.

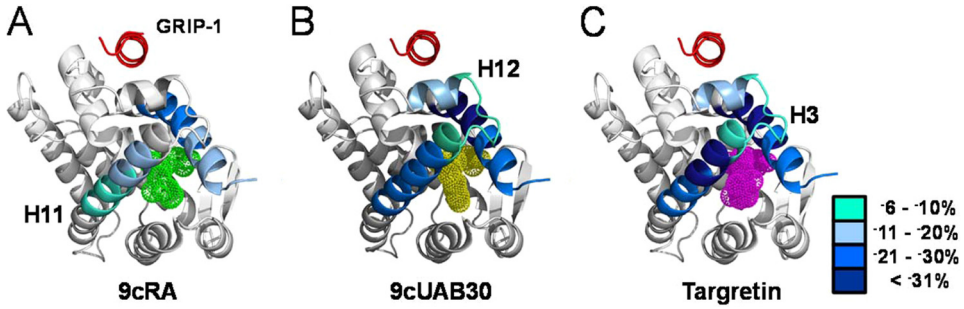

FIGURE 7. **HDX MS analyses mapped onto hRXRα-LBD·GRIP-1·agonist structures.** *A*, 9cRA; *B*, 9cUAB30; *C*, Targretin. Regions that show <5% difference in %D incorporation between agonist structures are *gray*. Regions that show >5% difference in %D are *colored* according to the heat map. Significant changes occur in H3, H11, and H12 regions and distinguish the two rexinoids from the pan-agonist 9cRA.

cant difference in the changes in %D for the H4 peptide between the three ligands as was the case for the majority of the observed HDX MS peptides.

The dynamical changes from all comparative HDX MS peptides with >5% change in %D were painted onto one monomer of the holo-hRXRα-LBD structures containing GRIP-1 (Fig. 7). (GRIP-1 is colored *red* and viewed along its helical axis in Fig. 7). The regions of change in %D for the two rexinoids mimic those found with 9cRA in the presence of GRIP-1 (12). However, H12 is stabilized by coactivator binding to hRXRα-LBD only when a rexinoid was present. GRIP-1 binding also stabilized H3 and the C terminus of H11. The largest effects were present when Targretin was present in the retinoid binding site. When 9cUAB30 was bound, the stabilization was slightly less than observed for Targretin but significantly larger than that when 9cRA was present.

We and others have shown that an increase in %D was observed for the H12 peptide when the hRXRα-LBD had bound retinoid but lacked coactivator peptide (10, 12, 47). This indicated that the dynamics of H12 residues increased for holo-hRXRα-LBD containing 9cRA over apo-hRXRα-LBD. Based on these previous results, we evaluated HDX MS of the holo-hRXRα-LBD complexes with the two rexinoids without coactivator peptide and used apo-hRXRα-LBD as the reference control. In the absence of GRIP-1, H12 peptides also showed a positive HDX perturbation (ranging from 6 to 13%) when hRXRα-LBD was bound with rexinoid only. The %D for H3 and H11 peptides was reduced relative to the reference control.

However, the extent of decrease in %D was dependent on retinoid compared with the analysis for this region when GRIP-1 was present. For example, the H3 Ala^{271}–Ala^{278} peptide displayed a −52% perturbation when 9cRA was bound to homodimers and a −30% perturbation when 9cUAB30 was bound. Likewise, for the H11 peptide Pro^{423}–Phe^{438}, the greatest HDX perturbations were found when homodimers were bound to Targretin (−27%) or 9cRA (−24%), but this reduction was smaller when 9cUAB30 was bound (−18%). Because H11 contains 21 residues, there were overlapping peptides that spanned smaller sections of this α-helix. Based on the peptide analysis of overlapping peptides, we pinpointed the C-terminal end of H11 (Ile^{428}–Phe^{438}) as the sequence whose HDX perturbations were dependent on agonist. A complete listing the HDX perturbations of hRXRα-LBD peptides is provided in supplemental Table S2.

DISCUSSION

We have demonstrated that 9cUAB30 compared well with Targretin in its capacity to prevent mammary cancer (21–25). The *in vitro* studies presented here also show how similar each rexinoid is in blocking ErbB2-oncogenic transformation, consistent with *in vivo* studies. At the molecular level, each rexinoid recruits the coactivator peptide GRIP-1 to the surface of its LBD in 1:1 stoichiometry. The thermodynamics for the formation of the coactivator complex with this NR are the same regardless of which rexinoid is bound to the LBD. We investigated the structures and dynamics of GRIP-1 binding to the holo-hRXRα-LBD complex with the rexinoid Targretin or 9cUAB30. Through our analysis of these two structures and our previously reported 9cRA structure, we identify four structural changes that occur when GRIP-1 binds to the holo-hRXRα-LBD·rexinoid complex that appear to be hallmarks of hRXRα-LBD agonist plus coactivator active conformations. These changes are as follows: 1) the carboxylate group of Asp^{273} (H3) forms a strong interaction with Thr^{449} and Phe^{450} of H12; 2) the phenyl ring of Phe^{277} (H3) forms a π-hydrogen bond with Phe^{450} (H12); 3) the guanidinium group of Arg^{302} (H4) forms ionic interactions with Glu^{453} and Glu^{456} of H12; and 4) H11 changes its helical axis by 10°, and Phe^{437} (H11) moves from a solvent-exposed environment to one that interacts with hydrophobic side chain carbon atoms on Leu^{455} on H12. These structural changes are very similar to those identified for this NR bound to 9cRA (18). Our comparative HDX MS analysis of hRXRα-LBD dynamics clearly show that these regions experience the greatest change in %D when both ligand and coactivator are bound, as is reflected in Fig. 7.

Based on these results, we examined if these four structural features were present in other RXR structures contained in the Protein Data Bank. Twenty-six structures of hRXRα-LBD were found (data not shown). For the 15 structures of hRXRα-LBD homodimers containing a bound agonist and a coactivator peptide (GRIP-1 or SCR-1), we found each of the four structural features listed above (12, 30, 48–55). Two structures were of hRXRα-LBD homodimers or tetramers with corepressor peptides bound (56), and the four interactions identified for coactivator binding with agonist were missing. In a similar manner, the crystal structures of apo-hRXRα-LBD homodimer (7) or apo-hRXRα-LBD tetramer (57) did not contain these interactions. These structures support the importance of each of these interactions in establishing a linkage between the agonist in the LBP and the coactivator binding site on the surface on the receptor.

The crystallographic structures of the coactivator peptide complex with holo-hRXRα-LBD (containing rexinoid or pan-agonist) are very similar. In contrast to these subtle structural changes, we made use of comparative HDX MS to reveal large changes in dynamics between these two structures. Three helices (H3, H11, and H12) in holo-hRXRα-LBD homodimers were stabilized when GRIP-1 bound to hRXRα-LBD containing either 9cUAB30 or Targretin. The dynamics of peptides corresponding to essentially all of the H11 residues (spanning Leu^{419}–Phe^{438}) were significantly reduced (up to 39%) with GRIP-1 binding (Fig. 6 and supplemental Table S1). H11 tilts by 10°, and Phe^{437} at its carboxyl end makes a major conformational change and swings toward the interior of the LBD. As shown in Fig. 4*B*, Phe^{437} is central to a molecular bridge that connects H12 residues (Leu^{455} and Glu^{456}) and residue His^{687} on the coactivator peptide GRIP-1 in one direction to the rexinoid ring in the other direction.

In light of this extensive change in H11 dynamics, we compared the contacts between the retinoid rings with H11 residues more closely. 9cRA interacts with H11 residues through its gem-dimethyl group on C1 (C16 and C17). We had reported that these interactions become more enhanced when coactivator peptide is present because the 9cRA ring rotates toward H11 on the GRIP-1-bound structure (18). (We previously reported that the trimethylcyclohexenyl ring inverts conformation, but we were in error.) Leu^{436}, Phe^{439}, His^{435}, and Cys^{432} make favorable van der Waals contacts with the gem-dimethyl groups of 9cRA (C16 and C17) (Fig. 5*A*). For 9cUAB30, the tetralone ring does not contain methyl substituents, but the six-member cyclohexenyl ring (C5, C6, C7, C2′, C1′, and C18 with an exocyclic double bond) interacts well with many H11 residues. In particular, the methylene groups of this ring (C2′, C1′, and C18) make substantial contact with the four H11 residues in the LBP (Fig. 5*C*; C2′ forms van der Waals contact with Leu^{436}, C1′ makes contact with Cys^{432}, and C18 interacts with Phe^{439}). For Targretin, the three methyl groups (C23, C24, and C25) contact H11 residues, but there is little contact from other carbon atoms in this ring. Targretin is more twisted in the LBP than the other two retinoids, and contact to H11 occurs only through these methyl groups (Fig. 5, *B–D*).

In addition to differences in H11 dynamics, we observed changes in dynamics for peptides containing Tyr^{249}–Leu^{279} residues. These residues are contained in the loop connecting H1 to H3 and the amino end of H3 (Fig. 2). (H2 is resolved in x-ray structures of apo-hRXRα-LBD, but it is unresolved in all holostructures.) This region of the LBD includes Asp^{273} and Phe^{277} (both on H3), which change conformation and establish another molecular bridge connecting the H12 residues and the retinoids. Unlike the bridge for H11 residues, Phe^{277} interacts strongly with Phe^{450} on H12, which is a key residue for forming the hydrophobic pocket of Ile^{689} and Leu^{693} in the IL*XX*LL motif of GRIP-1 (Fig. 4*B*). Asp^{273} on H3 forms a strong salt bridge with Arg^{302} on H4. Whereas H3 residues substantially

reduce dynamics upon GRIP-1 binding, the dynamics of H4 residues, including Arg^{302}, are already low, and they do not significantly change with GRIP-1 binding (Fig. 6*A*). Ile^{268}, Cys^{269}, Ala^{271}, and Ala^{272} on H3 are involved in forming the LBP for the rexinoids. Cys^{269} interacts very strongly with the C27 methyl group of Targretin, which occupies space that the other agonists do not (see Fig. 5, *C* and *D*). A conformational change occurs at the surface of the LBD receptor for Lys^{686} and Ile^{689} on GRIP-1 (Fig. 3, *B* and *C*), which may be communicated by this network of interactions.

H12 is necessary for recruitment of coactivator proteins and activation of transcription (58). Several studies of RXR activation have shown that H12 is not locked in a single active conformation, suggesting that H12 of RXR is only weakly influenced by the presence of the agonist (59, 60). For example, the structure of RXRβ bound by RXR-selective agonist LG268 showed that H12 did not adopt the active conformation when crystallized without coactivator (61). This is supported in our HDX MS studies of hRXRα-LBD dynamics. H12 stabilized only when GRIP-1 *and* rexinoids (Targretin or 9cUAB30) were present (Fig. 6 and supplemental Table S2). In contrast to the two rexinoids, the HDX MS analysis of the pan-agonist 9cRA binding clearly demonstrated that only GRIP-1 binding stabilizes H12 (12) and that 9cRA does not play a direct role (Fig. 6). Thus, our report provides the first evidence that retinoid agonists influence the H12 dynamics of hRXRα-LBD differently to recruit GRIP-1 coactivator peptide.

RXR tetramers form at physiologically relevant concentrations, and they are a transcriptionally silent form of the receptor (62). Tetramers dissociate into dimers upon ligand binding (63, 64). An mRXRΔH12 mutant does not have transcriptional activity, but it displays WT oligomeric activity (tetramer-dimer association), and cancer-relevant genes are up-regulated (65). Each of the regions of RXR LBD identified by their differential HDX MS profiles here (H3, H11, and H12) are important for RXR tetramer formation. The crystal structure of RXR tetramer demonstrated that the RXR tetrameric structure is stabilized by H11-H11 and H3-H3 interactions as well as interactions between the H12 AF-2 domain of one dimer and the coactivator binding groove of the other dimer (57). A recent tetramer structure that includes the silencing mediator for retinoid and thyroid hormone receptors (SMRT) and an antagonist, rhein, identified H3 and H11 in the autorepression of RXR (56). In fact, two key residues (Asp^{273} and Phe^{437}), which we propose connect the LBP and the coactivator, were also shown to stabilize the antagonist and corepressor in the tetramer. This would lead us to hypothesize that the structurally different rexinoid agonists may interact with H3 and H11 residues uniquely and destabilize the hRXRα tetramer at different rates.

Reduction in H3 and H11 dynamics in this NR is a hallmark of coactivator peptide recruitment by an agonist-bound LBD. HDX MS is often used to screen potential drug libraries and predict potency for NR agonist activity. The capacity for an agonist to stabilize H3 and H11 should be a reflection of its potency, which makes HDX a valuable drug screen. Because the reduced dynamics are dependent on both the presence of agonist *and* coactivator peptide, the results presented here indicate that drug libraries are best screened when coactivator peptides are included rather than the more common approach, which compares NR dynamics in the presence and absence of only agonist. Importantly, our HDX MS results clearly demonstrate that changes in dynamics upon ligand binding alone are not necessarily indicative of the changes observed when the coactivator is present.

This study integrates structural with dynamical analyses in order to understand the manner by which two RXR-selective agonists, Targretin and 9cUAB30, recruit the coactivator peptide GRIP-1 to the surface of the LBD. Although these two rexinoids have significantly different chemical structures, each fills the LBP of hRXRα-LBD and allows the LBD to fold to nearly identical tertiary structures in the presence of the GRIP-1 coactivator peptide in the x-ray crystal structures. A review of all x-ray structures with and without coactivator peptides bound to this NR LBD allows us to define four structural changes that form two molecular bridges that connect agonist and coactivator binding sites. These structural changes are hallmarks that define how agonist and coactivator binding stabilize H3, H11, and H12 and initiate transcription.

Acknowledgment—We thank Bruce Pascal for assistance with data analysis software.

REFERENCES

1. Kroenke, K., Arrington, M. E., and Mangelsdorff, A. D. (1990) The prevalence of symptoms in medical outpatients and the adequacy of therapy. *Arch. Intern. Med.* **150,** 1685–1689
2. Heyman, R. A., Mangelsdorf, D. J., Dyck, J. A., Stein, R. B., Eichele, G., Evans, R. M., and Thaller, C. (1992) 9-*cis*-retinoic acid is a high affinity ligand for the retinoid X receptor. *Cell* **68,** 397–406
3. Levin, A. A., Sturzenbecker, L. J., Kazmer, S., Bosakowski, T., Huselton, C., Allenby, G., Speck, J., Kratzeisen, C., Rosenberger, M., and Lovey, A. (1992) 9-*cis*-Retinoic acid stereoisomer binds and activates the nuclear receptor RXRα. *Nature* **355,** 359–361
4. Allegretto, E. A., McClurg, M. R., Lazarchik, S. B., Clemm, D. L., Kerner, S. A., Elgort, M. G., Boehm, M. F., White, S. K., Pike, J. W., and Heyman, R. A. (1993) Transactivation properties of retinoic acid and retinoid X receptors in mammalian cells and yeast. Correlation with hormone binding and effects of metabolism. *J. Biol. Chem.* **268,** 26625–26633
5. Allenby, G., Bocquel, M. T., Saunders, M., Kazmer, S., Speck, J., Rosenberger, M., Lovey, A., Kastner, P., Grippo, J. F., and Chambon, P. (1993) Retinoic acid receptors and retinoid X receptors. Interactions with endogenous retinoic acids. *Proc. Natl. Acad. Sci. U.S.A.* **90,** 30–34
6. Egea, P. F., Mitschler, A., Rochel, N., Ruff, M., Chambon, P., and Moras, D. (2000) Crystal structure of the human RXRα ligand-binding domain bound to its natural ligand: 9-*cis*-retinoic acid. *EMBO J.* **19,** 2592–2601
7. Bourguet, W., Ruff, M., Chambon, P., Gronemeyer, H., and Moras, D. (1995) Crystal structure of the ligand-binding domain of the human nuclear receptor RXR-α. *Nature* **375,** 377–382
8. Chalmers, M. J., Busby, S. A., Pascal, B. D., He, Y., Hendrickson, C. L., Marshall, A. G., and Griffin, P. R. (2006) Probing protein ligand interactions by automated hydrogen/deuterium exchange mass spectrometry. *Anal. Chem.* **78,** 1005–1014
9. Lu, J., Cistola, D. P., and Li, E. (2006) Analysis of ligand binding and protein dynamics of human retinoid X receptor α ligand-binding domain by nuclear magnetic resonance. *Biochemistry* **45,** 1629–1639
10. Yan, X., Broderick, D., Leid, M. E., Schimerlik, M. I., and Deinzer, M. L. (2004) Dynamics and ligand-induced solvent accessibility changes in human retinoid X receptor homodimer determined by hydrogen deuterium exchange and mass spectrometry. *Biochemistry* **43,** 909–917
11. Chalmers, M. J., Pascal, B. D., Willis, S., Zhang, J., Iturria, S. J., Dodge, J. A., and Griffin, P. R. (2011) Methods for the analysis of high precision differ-

ential hydrogen deuterium exchange data. *Int. J. Mass Spectrom.* **302,** 59–68
12. Xia, G., Boerma, L. J., Cox, B. D., Qiu, C., Kang, S., Smith, C. D., Renfrow, M. B., and Muccio, D. D. (2011) Structure, energetics, and dynamics of binding coactivator peptide to the human retinoid X receptor α ligand binding domain complex with 9-*cis*-retinoic acid. *Biochemistry* **50,** 93–105
13. Lehmann, J. M., Jong, L., Fanjul, A., Cameron, J. F., Lu, X. P., Haefner, P., Dawson, M. I., and Pfahl, M. (1992) Retinoids selective for retinoid X receptor response pathways. *Science* **258,** 1944–1946
14. Boehm, M. F., Zhang, L., Badea, B. A., White, S. K., Mais, D. E., Berger, E., Suto, C. M., Goldman, M. E., and Heyman, R. A. (1994) Synthesis and structure-activity relationships of novel retinoid X receptor-selective retinoids. *J. Med. Chem.* **37,** 2930–2941
15. Bischoff, E. D., Gottardis, M. M., Moon, T. E., Heyman, R. A., and Lamph, W. W. (1998) Beyond tamoxifen. The retinoid X receptor-selective ligand LGD1069 (TARGRETIN) causes complete regression of mammary carcinoma. *Cancer Res.* **58,** 479–484
16. Bischoff, E. D., Heyman, R. A., and Lamph, W. W. (1999) Effect of the retinoid X receptor-selective ligand LGD1069 on mammary carcinoma after tamoxifen failure. *J. Natl. Cancer Inst.* **91,** 2118
17. Gottardis, M. M., Bischoff, E. D., Shirley, M. A., Wagoner, M. A., Lamph, W. W., and Heyman, R. A. (1996) Chemoprevention of mammary carcinoma by LGD1069 (Targretin). An RXR-selective ligand. *Cancer Res.* **56,** 5566–5570
18. Lubet, R. A., Christov, K., Nunez, N. P., Hursting, S. D., Steele, V. E., Juliana, M. M., Eto, I., and Grubbs, C. J. (2005) Efficacy of Targretin on methylnitrosourea-induced mammary cancers. Prevention and therapy dose-response curves and effects on proliferation and apoptosis. *Carcinogenesis* **26,** 441–448
19. Duvic, M., Martin, A. G., Kim, Y., Olsen, E., Wood, G. S., Crowley, C. A., and Yocum, R. C. (2001) Phase 2 and 3 clinical trial of oral bexarotene (Targretin capsules) for the treatment of refractory or persistent early-stage cutaneous T-cell lymphoma. *Arch. Dermatol.* **137,** 581–593
20. Miller, V. A., Benedetti, F. M., Rigas, J. R., Verret, A. L., Pfister, D. G., Straus, D., Kris, M. G., Crisp, M., Heyman, R., Loewen, G. R., Truglia, J. A., and Warrell, R. P., Jr. (1997) Initial clinical trial of a selective retinoid X receptor ligand, LGD1069. *J. Clin. Oncol.* **15,** 790–795
21. Muccio, D. D., Brouillette, W. J., Breitman, T. R., Taimi, M., Emanuel, P. D., Zhang, X., Chen, G., Sani, B. P., Venepally, P., Reddy, L., Alam, M., Simpson-Herren, L., and Hill, D. L. (1998) Conformationally defined retinoic acid analogues. 4. Potential new agents for acute promyelocytic and juvenile myelomonocytic leukemias. *J. Med. Chem.* **41,** 1679–1687
22. Dawson, M. I., Jong, L., Hobbs, P. D., Cameron, J. F., Chao, W. R., Pfahl, M., Lee, M. O., Shroot, B., and Pfahl, M. (1995) Conformational effects on retinoid receptor selectivity. 2. Effects of retinoid bridging group on retinoid X receptor activity and selectivity. *J. Med. Chem.* **38,** 3368–3383
23. Grubbs, C. J., Lubet, R. A., Atigadda, V. R., Christov, K., Deshpande, A. M., Tirmal, V., Xia, G., Bland, K. I., Eto, I., Brouillette, W. J., and Muccio, D. D. (2006) Efficacy of new retinoids in the prevention of mammary cancers and correlations with short-term biomarkers. *Carcinogenesis* **27,** 1232–1239
24. Atigadda, V. R., Vines, K. K., Grubbs, C. J., Hill, D. L., Beenken, S. L., Bland, K. I., Brouillette, W. J., and Muccio, D. D. (2003) Conformationally defined retinoic acid analogues. 5. Large-scale synthesis and mammary cancer chemopreventive activity for (2E,4E,6Z,8E)-8-(3′,4′-dihydro-1′(2′H)-naphthalen-1′-ylidene)-3,7-dimethyl-2,4,6-octatrienoic acid (9cUAB30). *J. Med. Chem.* **46,** 3766–3769
25. Lindeblad, M., Kapetanovic, I. M., Kabirov, K. K., Dinger, N., Mankovskaya, I., Morrisey, R., Martín-Jiménez, T., and Lyubimov, A. (2011) Assessment of oral toxicity and safety of 9-cis-UAB30, a potential chemopreventive agent, in rat and dog studies. *Drug Chem. Toxicol.* **34,** 300–310
26. Vedell, P. T., Lu, Y., Grubbs, C. J., Yin, Y., Jiang, H., Bland, K. I., Muccio, D. D., Cvetkovic, D., You, M., and Lubet, R. (2013) Effects on gene expression in rat liver after administration of RXR agonists. UAB30, 4-methyl-UAB30, and Targretin (Bexarotene). *Mol. Pharmacol.* **83,** 698–708
27. Kolesar, J. M., Hoel, R., Pomplun, M., Havighurst, T., Stublaski, J., Wollmer, B., Krontiras, H., Brouillette, W., Muccio, D., Kim, K., Grubbs, C. J., and Bailey, H. E. (2010) A pilot, first-in-human, pharmacokinetic study of 9cUAB30 in healthy volunteers. *Cancer Prev. Res.* (*Phila.*) **3,** 1565–1570
28. Jiang, W., Deng, W., Bailey, S. K., Nail, C. D., Frost, A. R., Brouillette, W. J., Muccio, D. D., Grubbs, C. J., Ruppert, J. M., and Lobo-Ruppert, S. M. (2009) Prevention of KLF4-mediated tumor initiation and malignant transformation by UAB30 rexinoid. *Cancer Biol. Ther.* **8,** 289–298
29. Egea, P. F., and Moras, D. (2001) Purification and crystallization of the human RXRα ligand-binding domain-9-cisRA complex. *Acta Crystallogr. D Biol. Crystallogr.* **57,** 434–437
30. Egea, P. F., Mitschler, A., and Moras, D. (2002) Molecular recognition of agonist ligands by RXRs. *Mol. Endocrinol.* **16,** 987–997
31. Sobolev, V., Sorokine, A., Prilusky, J., Abola, E. E., and Edelman, M. (1999) Automated analysis of interatomic contacts in proteins. *Bioinformatics* **15,** 327–332
32. Kleywegt, G. J., and Jones, T. A. (1994) Detection, delineation, measurement and display of cavities in macromolecular structures. *Acta Crystallogr. D Biol. Crystallogr.* **50,** 178–185
33. Kleywegt, G. J., and Jones, T. A. (1996) xdlMAPMAN and xdlDATAMAN. Programs for reformatting, analysis and manipulation of biomacromolecular electron-density maps and reflection data sets. *Acta Crystallogr. D Biol. Crystallogr.* **52,** 826–828
34. Pascal, B. D., Chalmers, M. J., Busby, S. A., and Griffin, P. R. (2009) HD desktop. An integrated platform for the analysis and visualization of H/D exchange data. *J. Am. Soc. Mass Spectrom.* **20,** 601–610
35. Kang, S., Poliakov, A., Sexton, J., Renfrow, M. B., and Prevelige, P. E., Jr. (2008) Probing conserved helical modules of portal complexes by mass spectrometry-based hydrogen/deuterium exchange. *J. Mol. Biol.* **381,** 772–784
36. Ascano, J. M., Beverly, L. J., and Capobianco, A. J. (2003) The C-terminal PDZ-ligand of JAGGED1 is essential for cellular transformation. *J. Biol. Chem.* **278,** 8771–8779
37. Capobianco, A. J., Zagouras, P., Blaumueller, C. M., Artavanis-Tsakonas, S., and Bishop, J. M. (1997) Neoplastic transformation by truncated alleles of human NOTCH1/TAN1 and NOTCH2. *Mol. Cell. Biol.* **17,** 6265–6273
38. Foster, K. W., Ren, S., Louro, I. D., Lobo-Ruppert, S. M., McKie-Bell, P., Grizzle, W., Hayes, M. R., Broker, T. R., Chow, L. T., and Ruppert, J. M. (1999) Oncogene expression cloning by retroviral transduction of adenovirus E1A-immortalized rat kidney RK3E cells. Transformation of a host with epithelial features by c-MYC and the zinc finger protein GKLF. *Cell Growth Differ.* **10,** 423–434
39. Kolligs, F. T., Hu, G., Dang, C. V., and Fearon, E. R. (1999) Neoplastic transformation of RK3E by mutant β-catenin requires deregulation of Tcf/Lef transcription but not activation of c-myc expression. *Mol. Cell. Biol.* **19,** 5696–5706
40. Jung, D., Inagaki, T., Gerard, R. D., Dawson, P. A., Kliewer, S. A., Mangelsdorf, D. J., and Moschetta, A. (2007) FXR agonists and FGF15 reduce fecal bile acid excretion in a mouse model of bile acid malabsorption. *J. Lipid Res.* **48,** 2693–2700
41. Rahman, L., Voeller, D., Rahman, M., Lipkowitz, S., Allegra, C., Barrett, J. C., Kaye, F. J., and Zajac-Kaye, M. (2004) Thymidylate synthase as an oncogene. A novel role for an essential DNA synthesis enzyme. *Cancer Cell* **5,** 341–351
42. Tonon, G., Modi, S., Wu, L., Kubo, A., Coxon, A. B., Komiya, T., O'Neil, K., Stover, K., El-Naggar, A., Griffin, J. D., Kirsch, I. R., and Kaye, F. J. (2003) t(11;19)(q21;p13) translocation in mucoepidermoid carcinoma creates a novel fusion product that disrupts a Notch signaling pathway. *Nat. Genet.* **33,** 208–213
43. Foster, K. W., Liu, Z., Nail, C. D., Li, X., Fitzgerald, T. J., Bailey, S. K., Frost, A. R., Louro, I. D., Townes, T. M., Paterson, A. J., Kudlow, J. E., Lobo-Ruppert, S. M., and Ruppert, J. M. (2005) Induction of KLF4 in basal keratinocytes blocks the proliferation-differentiation switch and initiates squamous epithelial dysplasia. *Oncogene* **24,** 1491–1500
44. Rocha, G. M., Michea, L. F., Peters, E. M., Kirby, M., Xu, Y., Ferguson, D. R., and Burg, M. B. (2001) Direct toxicity of nonsteroidal antiinflammatory drugs for renal medullary cells. *Proc. Natl. Acad. Sci. U.S.A.* **98,** 5317–5322
45. Ghosh, J. C., Yang, X., Zhang, A., Lambert, M. H., Li, H., Xu, H. E., and

Chen, J. D. (2002) Interactions that determine the assembly of a retinoid X receptor/corepressor complex. *Proc. Natl. Acad. Sci. U.S.A.* **99,** 5842–5847
46. Dai, S. Y., Chalmers, M. J., Bruning, J., Bramlett, K. S., Osborne, H. E., Montrose-Rafizadeh, C., Barr, R. J., Wang, Y., Wang, M., Burris, T. P., Dodge, J. A., and Griffin, P. R. (2008) Prediction of the tissue-specificity of selective estrogen receptor modulators by using a single biochemical method. *Proc. Natl. Acad. Sci. U.S.A.* **105,** 7171–7176
47. Zhang, J., Chalmers, M. J., Stayrook, K. R., Burris, L. L., Wang, Y., Busby, S. A., Pascal, B. D., Garcia-Ordonez, R. D., Bruning, J. B., Istrate, M. A., Kojetin, D. J., Dodge, J. A., Burris, T. P., and Griffin, P. R. (2011) DNA binding alters coactivator interaction surfaces of the intact VDR-RXR complex. *Nat. Struct. Mol. Biol.* **18,** 556–563
48. le Maire, A., Bourguet, W., and Balaguer, P. (2010) A structural view of nuclear hormone receptor. Endocrine disruptor interactions. *Cell. Mol. Life Sci.* **67,** 1219–1237
49. le Maire, A., Grimaldi, M., Roecklin, D., Dagnino, S., Vivat-Hannah, V., Balaguer, P., and Bourguet, W. (2009) Activation of RXR-PPAR heterodimers by organotin environmental endocrine disruptors. *EMBO Rep.* **10,** 367–373
50. Lippert, W. P., Burschka, C., Götz, K., Kaupp, M., Ivanova, D., Gaudon, C., Sato, Y., Antony, P., Rochel, N., Moras, D., Gronemeyer, H., and Tacke, R. (2009) Silicon analogues of the RXR-selective retinoid agonist SR11237 (BMS649). Chemistry and biology. *ChemMedChem* **4,** 1143–1152
51. Nahoum, V., Pérez, E., Germain, P., Rodríguez-Barrios, F., Manzo, F., Kammerer, S., Lemaire, G., Hirsch, O., Royer, C. A., Gronemeyer, H., de Lera, A. R., and Bourguet, W. (2007) Modulators of the structural dynamics of the retinoid X receptor to reveal receptor function. *Proc. Natl. Acad. Sci. U.S.A.* **104,** 17323–17328
52. Pérez Santín, E., Germain, P., Quillard, F., Khanwalkar, H., Rodríguez-Barrios, F., Gronemeyer, H., de Lera, A. R., and Bourguet, W. (2009) Modulating retinoid X receptor with a series of (*E*)-3-[4-hydroxy-3-(3-alkoxy-5,5,8,8-tetramethyl-5,6,7,8-tetrahydronaphthalen-2-yl)phenyl]acrylic acids and their 4-alkoxy isomers. *J. Med. Chem.* **52,** 3150–3158
53. Zhang, H., Li, L., Chen, L., Hu, L., Jiang, H., and Shen, X. (2011) Structure basis of bigelovin as a selective RXR agonist with a distinct binding mode. *J. Mol. Biol.* **407,** 13–20
54. Zhang, H., Xu, X., Chen, L., Chen, J., Hu, L., Jiang, H., and Shen, X. (2011) Molecular determinants of magnolol targeting both RXRα and PPARγ. *PLoS One* **6,** e28253
55. Zhang, Y., Zhang, H., Yao, X. G., Shen, H., Chen, J., Li, C., Chen, L., Zheng, M., Ye, J., Hu, L., Shen, X., and Jiang, H. (2012) (+)-Rutamarin as a dual inducer of both GLUT4 translocation and expression efficiently ameliorates glucose homeostasis in insulin-resistant mice. *PLoS One* **7,** e31811
56. Zhang, H., Chen, L., Chen, J., Jiang, H., and Shen, X. (2011) Structural basis for retinoic X receptor repression on the tetramer. *J. Biol. Chem.* **286,** 24593–24598
57. Gampe, R. T., Jr., Montana, V. G., Lambert, M. H., Wisely, G. B., Milburn, M. V., and Xu, H. E. (2000) Structural basis for autorepression of retinoid X receptor by tetramer formation and the AF-2 helix. *Genes Dev.* **14,** 2229–2241
58. Barroso, I., Gurnell, M., Crowley, V. E., Agostini, M., Schwabe, J. W., Soos, M. A., Maslen, G. L., Williams, T. D., Lewis, H., Schafer, A. J., Chatterjee, V. K., and O'Rahilly, S. (1999) Dominant negative mutations in human PPARγ associated with severe insulin resistance, diabetes mellitus and hypertension. *Nature* **402,** 880–883
59. Renaud, J. P., Rochel, N., Ruff, M., Vivat, V., Chambon, P., Gronemeyer, H., and Moras, D. (1995) Crystal structure of the RAR-γ ligand-binding domain bound to all-*trans*-retinoic acid. *Nature* **378,** 681–689
60. Lin, B. C., Hong, S. H., Krig, S., Yoh, S. M., and Privalsky, M. L. (1997) A conformational switch in nuclear hormone receptors is involved in coupling hormone binding to corepressor release. *Mol. Cell. Biol.* **17,** 6131–6138
61. Love, J. D., Gooch, J. T., Benko, S., Li, C., Nagy, L., Chatterjee, V. K., Evans, R. M., and Schwabe, J. W. (2002) The structural basis for the specificity of retinoid-X receptor-selective agonists. New insights into the role of helix H12. *J. Biol. Chem.* **277,** 11385–11391
62. Kersten, S., Kelleher, D., Chambon, P., Gronemeyer, H., and Noy, N. (1995) Retinoid X receptor α forms tetramers in solution. *Proc. Natl. Acad. Sci. U.S.A.* **92,** 8645–8649
63. Kersten, S., Pan, L., Chambon, P., Gronemeyer, H., and Noy, N. (1995) Role of ligand in retinoid signaling. 9-*cis*-retinoic acid modulates the oligomeric state of the retinoid X receptor. *Biochemistry* **34,** 13717–13721
64. Kersten, S., Pan, L., and Noy, N. (1995) On the role of ligand in retinoid signaling. Positive cooperativity in the interactions of 9-*cis*-retinoic acid with tetramers of the retinoid X receptor. *Biochemistry* **34,** 14263–14269
65. Yasmin, R., Kannan-Thulasiraman, P., Kagechika, H., Dawson, M. I., and Noy, N. (2010) Inhibition of mammary carcinoma cell growth by RXR is mediated by the receptor's oligomeric switch. *J. Mol. Biol.* **397,** 1121–1131